Synergism of dual AAV gene therapy and rapamycin rescues GSDIII phenotype in muscle and liver

Louisa Jauze, … , Xavier Nissan, Giuseppe Ronzitti

Research In-Press Preview **Therapeutics**

Glycogen storage disease type III (GSDIII) is a rare metabolic disorder due to glycogen debranching enzyme (GDE) deficiency. Reduced GDE activity leads to pathological glycogen accumulation responsible for impaired hepatic metabolism and muscle weakness. To date, there is no curative treatment for GSDIII. We previously reported that two distinct dual AAV vectors encoding for GDE were needed to correct liver and muscle in a GSDIII mouse model. Here, we evaluated the efficacy of rapamycin in combination with AAV gene therapy. Simultaneous treatment with rapamycin and a novel dual AAV vector expressing GDE in the liver and muscle resulted in a synergic effect demonstrated at biochemical and functional levels. Transcriptomic analysis confirmed synergy and suggested a putative mechanism based on the correction of lysosomal impairment. In GSDIII mice liver, dual AAV gene therapy combined with rapamycin reduced the impact of the immune response to AAV observed in this disease model. These data provide proof of concept of an approach exploiting the combination of gene therapy and rapamycin to improve efficacy and safety and support clinical translation.

Find the latest version:

Synergism of dual AAV gene therapy and rapamycin rescues GSDIII phenotype in muscle and liver

L. Jauze[1,2,*], M. Vie[1,2,*], Q. Miagoux[3], L. Rossiaud[1,2,3], P. Vidal[1,2], V. Montalvo-Romeral[1,2], H. Saliba[1,2], M. Jarrige[3], H. Polveche[3], J. Nozi[1,2], P. Le Brun[1], J. Cosette[1], L. Bocchialini[1,2], A. Francois[1,2], J. Rouillon[1,2], F. Collaud[1,2], F. Bordier[1], E. Bertil-Froidevaux[1], C. Georger[1], L. van Wittenberghe[1], A. Miranda[1], N. Daniele[1], D.A. Gross[1,2], L. Hoch[3], X. Nissan[3], G. Ronzitti[1,2,†]

[1]Genethon, 91000 Evry, France

[2]Université Paris-Saclay, Univ Evry, Inserm, Genethon, Integrare research unit UMR_S951, 91000 Evry, France

[3]CECS, I-STEM, Institute for Stem Cell Therapy and Exploration of Monogenic Diseases, 28 rue Henri Desbruères, 91100 Corbeil-Essonnes, France.

* Equally contributed

† Corresponding author:

Giuseppe Ronzitti, PhD,

INSERM U951 ''INTEGRARE'', Genethon, Univ Evry, Université Paris-Saclay, 1bis rue De l'Internationale 91000 Evry, France; tel/fax: +33169472990; email: gronzitti@genethon.fr

ABSTRACT

Glycogen storage disease type III (GSDIII) is a rare metabolic disorder due to glycogen debranching enzyme (GDE) deficiency. Reduced GDE activity leads to pathological glycogen accumulation responsible for impaired hepatic metabolism and muscle weakness. To date, there is no curative treatment for GSDIII.

We previously reported that two distinct dual AAV vectors encoding for GDE were needed to correct liver and muscle in a GSDIII mouse model.

Here, we evaluated the efficacy of rapamycin in combination with AAV gene therapy. Simultaneous treatment with rapamycin and a novel dual AAV vector expressing GDE in liver and muscle resulted in a synergic effect demonstrated at biochemical and functional levels. Transcriptomic analysis confirmed synergy and suggested a putative mechanism based on the correction of lysosomal impairment. In GSDIII mice liver, dual AAV gene therapy combined with rapamycin reduced the impact of the immune response to AAV observed in this disease model.

These data provide proof of concept of an approach exploiting the combination of gene therapy and rapamycin to improve efficacy and safety and support clinical translation.

INTRODUCTION

Glycogen storage disease type III (GSDIII) is a rare, autosomal recessive disorder with an incidence of 1 in 100 000 live births due to mutations in the amylo-α-1, 6-glucosidase, 4-α-glucanotransferase gene (*AGL*). *AGL* encodes for the glycogen debranching enzyme (GDE). Its deficiency leads to glycogen accumulation mainly in liver, heart, and skeletal muscles. Inactivating mutations on the *AGL* gene result in impaired liver metabolism with severe hypoglycemia, heart function degradation, and progressive muscle weakness (1).

The disease evolves in two phases: i) in childhood, the main manifestation is the metabolic disorder with hepatomegaly, fasting hypoglycemia, hyperlipidemia, and hyperketonemia; ii) with aging, a progressive myopathy characterized by skeletal muscle weakness and exercise intolerance appears (2) together with a progressive liver disease (1, 3, 4). GSDIII patients also present cardiac involvement since early ages, in some cases associated with cardiomyopathy (2, 5).

To date, there is no curative treatment for GSDIII. A dietary regimen including frequent meals and a strict diet enriched in uncooked cornstarch, while controlling hypoglycemia episodes and reducing glycogen accumulation, fails at addressing the muscle impairment (1, 2, 6). High-protein diet were sporadically reported to be beneficial in reducing or stabilizing skeletal and cardiac muscle manifestations (7-12).

The unmet medical need and the fact that GSDIII has a monogenic origin make this disease an ideal target for gene replacement therapy. Adeno-associated virus (AAV)-derived vectors demonstrated efficient targeting of liver and muscle in multiple glycogenosis preclinical models (13-21). The limited packaging capacity of AAVs has been extended by demonstrating the feasibility of the use of two overlapping vectors encoding GDE in a mouse model of GSDIII (22).

Recently an orthogonal approach was described based on a single AAV vector encoding a bacterial GDE named pullulanase (23). When expressed under the control of a CMV enhancer/chicken β-actin promoter (CB), pullulanase corrected glycogen accumulation in skeletal muscle and heart, but not in

liver of a GSDIII mouse model. Injection of a second vector expressing pullulanase under the control of a liver specific promoter (LSP) in the same animals was necessary to correct the hepatic glycogen accumulation and reverse the hepatic fibrosis (23). However, the expression of pullulanase was lost after a few weeks probably because of transgene-induced cytotoxic T lymphocyte (24). To address this issue, a vector encoding pullulanase under a tandem promoter CB-LSP was assessed (24). The CB-LSP-pullulanase vector corrected glycogen accumulation in liver, heart, and quadriceps, reversed hepatic fibrosis, and decreased pullulanase-induced CTL response in GSDIII mice (24). Although promising, these data confirm the potential risk of immune responses to bacterial transgenes (25) that may preclude a clinical translation of this approach.

Here, in an effort to optimize the dual vector approach for GSDIII, we attempted the use of a recently developed tandem promoter expressing GDE in liver and muscles (AAV9-LiMP-GDEov). Despite transient rescue obtained after one month of treatment, the correction was lost overtime. To overcome this issue, and because rapamycin was shown to be promising for GSDIII treatment in a dog model of GSDIII (26), we assessed the efficiency of rapamycin alone and in combination with AAV9-LiMP-GDEov in a murine model of the disease. One-month treatment with rapamycin alone was not efficient in correcting the hepatic and muscular impairment in our mouse model. However, the same rapamycin treatment followed by the injection of AAV9-LiMP-GDEov had a synergic effect with gene therapy, increasing glycogen clearance in skeletal muscles and improving muscle strength rescue as compared to AAV9-LiMP-GDEov alone. This synergic effect was confirmed also by analyzing the RNA expression profile in triceps. In general, we observed a better rescue of the disease markers in animals treated with the combination of rapamycin and gene therapy. More precisely, the lysosomal pathway was better corrected in triceps of GSDIII mice treated with the combination therapy. Interestingly, transcriptomic analysis performed in the liver showed, in animals receiving the AAV9-LiMP-GDE vector, an RNA expression pattern suggestive of an immune response to gene therapy that was controlled by rapamycin treatment.

RESULTS

Long-term partial correction of the muscular and hepatic GSDIII phenotype in *Agl*^{-/-} mice with a dual AAV vector expressing GDE under the control of a tandem liver-muscle promoter.

We have previously established proof-of-concept of the correction of the muscular and hepatic disease manifestations in *Agl*^{-/-} mice with two distinct overlapping AAV vectors expressing GDE either under the control of a constitutive promoter or a liver-specific promoter (22). Although the CAG promoter allowed efficient expression of the GDE transgene in liver and muscle with a dual AAV vector, the use of such promoter was associated with an increased risk of immune response to the transgene (13, 27) and the potential formation of liver tumors at high vector doses when injected in neonatal animals (29).

To overcome these limitations and achieve safe and efficient gene transfer in both liver and muscle, we took advantage of a recently developed tandem liver-muscle promoter (LiMP) which allows us to control immune responses to the transgene while achieving a robust and specific expression in liver and muscle (13). Three-month-old *Agl*^{-/-} mice received 6×10^{13} vg/kg of a dual AAV9 vector expressing the human GDE transgene under the control of the LiMP (AAV9-LiMP-GDEov) and were followed-up for twelve months (**Figure 1A**). At sacrifice, Western blot analysis showed expression of GDE in heart, and quadriceps (**Figure 1B**). In the heart, the robust GDE expression, likely due to the high tissue transduction achieved with AAV9 (**Supplementary Table 1**), resulted in a partial correction of glycogen accumulation and histological features as measured biochemically and by hematoxylin-eosin (HE) and periodic-acid-Schiff (PAS) staining (**Figure 1C and Supplementary Figure 1A**). The lower transduction levels (**Supplementary Table 1**) and GDE protein expression (**Figure 1B**) correlated with partial correction of glycogen accumulation in quadriceps and triceps (**Figure 1C**). Those results were confirmed by HE and PAS staining that showed an only partial rescue of the histological features in quadriceps (**Figure 1D**). In liver, GDE transgene expression (**Figure 1E**) resulted in partial correction of glycogen accumulation (**Figure 1F**), with little to no effect on fibrosis, and other histological features

(**Supplementary Figure 1B**). Accordingly, at sacrifice, hepatomegaly was not corrected (**Figure 1G**). Surprisingly, one month after treatment of *Agl*$^{-/-}$ mice with AAV9-LiMP-GDEov, glycemia was completely corrected, whereas twelve months after vector injection the glycemia was no longer rescued (**Figure 1H**) confirming the biochemical data and supporting the hypothesis of a loss of correction in the liver. Evaluation of muscle function by wire-hang revealed a partial correction of the muscle strength impairment at both 1 and 12 months after AAV9-LiMP-GDEov administration (**Figure 1I**), suggesting stability of gene transfer over 12 months. Importantly, in mice treated with AAV9-LiMP-GDEov variable levels of anti-GDE antibodies were measured during the protocol that were not correlated with transgene expression levels in liver and muscle (**Supplementary Figure 1C**).

To conclude, long-term evaluation of the efficacy of an AAV gene therapy approach for GSDIII based on the use of a promoter with dual liver muscle specificity indicates partial rescue of muscle impairment and loss of efficacy in liver thus supporting the need for optimization to achieve full correction of GSDIII disease manifestations while reducing anti-transgene immunogenicity.

Pharmacological treatment with rapamycin alone does not correct the hepatic and muscular phenotype of *Agl*$^{-/-}$ mice.

Inhibition of the mammalian target of rapamycin (mTOR) leads to increased autophagy in multiple cell types. Inhibition of mTOR in immune cells is associated with decreased activation and immunosuppression (30). Although in GSDIII the pathological glycogen accumulation occurs in the cytosol, the activation of glycogen-specific autophagy (glycophagy) may participate in glycogen clearance. Moreover, it has been recently shown that autophagy is impaired in GSDIII skeletal muscle biopsies (31). Treatment with rapamycin was shown effective in a dog model of GSDIII, correcting glycogen accumulation in liver and preventing glycogen accumulation in skeletal muscle (26). To confirm these results in a mouse model of GSDIII, we treated symptomatic, 6-month-old *Agl*$^{-/-}$ mice with 1.5 mg/kg/day for one month, a regimen known to achieve immunosuppression in rodents (32)

(**Figure 2A**). After one month of daily treatment, we observed a slight increase in glycogen content in liver, heart, and skeletal muscles (**Figure 2B** and **Supplementary Figure 2A**). Together with no correction of hypoglycemia by rapamycin treatment (**Figure 2C**), we observed a tendency toward increased liver weight (**Figure 2D**). To rule out a potential toxicity due to rapamycin treatment, aspartate and alanine transaminases (AST and ALT) were measured in blood. The hepatic enzymes, elevated in $Agl^{-/-}$ mice, were not significantly increased by rapamycin treatment (**Supplementary Figures 2B, C**). Liver histological features were similar between the two groups of $Agl^{-/-}$ mice regardless of the treatment (**Figure 2E**), although tendentially decreased CD8+ infiltrates were measured in rapamycin-treated $Agl^{-/-}$ mice by histology and *CD8* mRNA analysis (**Supplementary Figure 2D-F**).

The general architecture of heart and skeletal muscle evaluated by HE and PAS staining showed signs of glycogen accumulation characteristic of the disease (**Figure 2F** and **Supplementary Figure 2G**).

Rapamycin is an mTOR inhibitor, however in the context of Pompe disease, another GSD, it has been shown that rapamycin may inhibit glycogen synthase in muscle (33). To test whether rapamycin was acting through the same mechanism, we evaluated the effect of a one-month treatment with the molecule on GSDIII mice. Gys1 inhibition was then assessed by measuring both total levels of Gys1, the muscle-specific glycogen synthase, and its Ser641 phosphorylation, a known inhibiting phosphorylation participating in the rapamycin effect observed in Pompe disease (33). We found that Gys1 was strongly inhibited in the triceps of $Agl^{-/-}$ mice while one-month treatment with rapamycin had no impact (**Supplementary Figures 2H,I**).

To evaluate the impact of rapamycin treatment on autophagy induction, we measured the levels of p62 protein, a known marker of autophagy in GSDs (31, 34, 35), in liver and muscle. In liver, p62 protein levels were increased in untreated $Agl^{-/-}$ mice compared to $Agl^{+/+}$, and only slightly decreased by rapamycin treatment (**Figure 2G**) suggesting a pre-existing block of hepatic autophagy in $Agl^{-/-}$ mice. Surprisingly, p62 levels in triceps of untreated $Agl^{-/-}$ mice were similar to those of wild-type animals and were greatly increased by rapamycin treatment (**Figure 2G**). Measurement of GAA activity in the

8

same tissue showed similar levels in $Agl^{+/+}$ and $Agl^{-/-}$ mice and treatment with rapamycin had no effect (**Supplementary Figures 2J**). Our current working hypothesis to interpretate the data obtained in skeletal muscle is described in **Supplementary Figure 3**. We hypothesize that rapamycin treatment increases the autophagic flux in GSDIII muscle leading to increased glycophagy. However, the lysosomal capacity to degrade glycogen remains constant as showed by the stable GAA activity and this leads to an accumulation of autophagosomes and the consequent increased p62 levels suggestive of an autophagy block.

Combination of rapamycin treatment with AAV9-LiMP-GDEov rescues liver and muscle phenotype in GSDIII mice.

In our experimental conditions, rapamycin treatment alone was not sufficient to clear glycogen in liver and muscle of GSDIII mice. We then tested whether autophagy induction with rapamycin treatment may synergize with the GDE enzyme expression achieved by gene transfer with AAV9-LiMP-GDEov. Symptomatic, six-month-old $Agl^{-/-}$ mice were treated daily for one month with 1.5 mg/kg/day of rapamycin before the injection of the AAV9-LiMP-GDEov vector, followed by additional fifteen days of the same rapamycin treatment. (**Figure 3A**). Three months after AAV injection, robust transduction levels and GDE expression were detected in liver of $Agl^{-/-}$ mice treated with AAV9-LiMP-GDEov regardless of the combined treatment (**Supplementary Table 1** and **Figure 3B**). Of note, differently from previous reports (36-38), rapamycin pretreatment did not improve AAV liver transduction in $Agl^{-/-}$ mice. Consistently, similar correction of glycogen accumulation and histological features was achieved in the liver in the two groups (**Figure 3C** and **Supplementary Figure 4A**). The lower glycemia values in $Agl^{-/-}$ mice measured at the start of the rapamycin treatment were corrected 3 months after AAV injection (**Supplementary Figure 4B**). Despite complete liver glycogen clearance and glycemia rescue the liver weight was not corrected in AAV9-LiMP-GDEov-treated animals regardless of the use of rapamycin (**Supplementary Figure 4C**). In the heart, transduction efficacy, GDE expression, partial

glycogen clearance and correction of the histological features were similar between *Agl^-/-* mice treated with AAV9-LiMP-GDEov with or without rapamycin (**Supplementary Table 1, Supplementary Figures 4D** and **Figures 3D,E**). Importantly, despite similar transduction (**Supplementary Table 1**), the combination of rapamycin with AAV9-LiMP-GDEov treatment led to increased GDE expression in quadriceps and in triceps (**Figure 3D**). Increased GDE expression in skeletal muscle resulted in a better glycogen clearance in the quadriceps and triceps of *Agl^-/-* mice treated with the combination of rapamycin and AAV9-LiMP-GDEov (**Figure 3E**). Accordingly, the histological features as measured by HE and PAS staining were better corrected in quadriceps and triceps of animals treated with the combination of rapamycin and gene therapy than gene therapy alone (**Figure 3F**). The better glycogen clearance and the normalization of the muscle histology resulted in a better correction of the muscle strength as assessed by wire hang in mice that received the combined treatment (**Figure 3G**).

Finally, in accordance with what was previously reported, the rapamycin treatment used decreased the level of anti-AAV9 IgG measured all along the protocol. Interestingly, the low levels of anti-GDE IgG measured after AAV vector injection were not affected by the treatment possibly due to the delayed kinetic of the anti-transgene immunity (**Supplementary Figure 4E**).

Combination of rapamycin treatment with AAV9-LiMP-GDEov rescues the disease's molecular signature of the muscle phenotype in GSDIII mice.

To further evaluate the correction of the muscle phenotype at a molecular level, we performed a transcriptomic analysis in triceps of *Agl^-/-* mice treated with AAV9-LiMP-GDEov with or without rapamycin. We identified a total of 217 differentially expressed genes (DEGs) among the different conditions. Among them, 207 were modified in vehicle-treated *Agl^-/-* mice and most of them were rescued by the treatment with AAV9-LiMP-GDEov (**Supplementary Table 2**). To examine gene expression patterns, a heatmap of DEGs was constructed (**Supplementary Figure 5A**). The findings suggested that the transcriptomic profile of *Agl^-/-* mice treated with combined gene therapy and

rapamycin was closer to PBS-treated *Agl*^+/+^ mice than the profile of AAV9-LiMP-GDEov-treated animals (**Supplementary Figure 5A**) thus supporting the synergic effect observed at both biochemical and functional levels (**Figure 3**). Validation of 5 upregulated and 4 downregulated genes was performed in triceps and liver showing a similar pattern of expression than RNAseq data (**Supplementary Table 3** and **4**).

To further characterize this synergism, we performed a Gene Set Enrichment Analysis with the Kyoto Encyclopedia of Genes and Genomes set of pathways (GSEA-KEGG) analysis in triceps. We identified 66 pathways significantly dysregulated between untreated *Agl*^+/+^ and *Agl*^-/-^ animals (**Figure 4A**). Among these pathways, 24 were rescued in AAV9-LiMP-GDEov-treated animals regardless of the combination with rapamycin (**Supplementary Figure 5B**). Twenty-one additional pathways were rescued only when the dual AAV vector was combined with the immunomodulatory drug further supporting the synergic effect of rapamycin and AAV9-LiMP-GDEov (**Figure 4A,B**). Importantly, "Lysosome'' was among the pathways modified only by the combined treatment (**Figure 4B**). Given the fundamental role of lysosomes in autophagy and the recent report of a autophagy impairment in muscles from patients' biopsies and GSDIII mice (31), we decided to characterize in detail the effect of the combined treatment on this pathway. To demonstrate the synergic effect of rapamycin and AAV9-LiMP-GDEov, we also included in this analysis a group of *Agl*^-/-^ mice treated with rapamycin. K-means clustering of the genes belonging to the "Lysosome'' pathway as defined in KEGG allowed us to group the genes of this family based on their profile in three main groups: i) modified by the treatment (i.e. those genes similar in *Agl*^+/+^ and *Agl*^-/-^ mice, unmodified by the disease), ii) modified by the disease and not rescued and, iii) modified by the disease and rescued (**Figure 4C**). Importantly, mice treated with the combination of AAV9-LiMP-GDEov and rapamycin had 58% of the gene in the category modified by the disease, rescued, while only 23% of the genes not rescued. A lower percentage of rescued genes was observed in the lysosomal pathway measured in *Agl*^-/-^ mice treated with rapamycin alone (30%) or with AAV9-LiMP-GDEov gene therapy alone (43%, **Figure 4D** and **Supplementary Table 5**). Visualization of the lysosomal pathway by Pathview showed that most of the genes modified in *Agl*^-/-^ mice in this

pathway were rescued by the combined treatment, further supporting the synergic effect of the two treatments for the rescue of this pathway (**Figures 5** and **6, Supplementary Table 6**).

To functionally validate the results obtained by RNA-seq, we explored more in detail the pathways of global autophagy. First, we measured acid alpha-glucosidase (GAA) activity in triceps, which was unchanged in $Agl^{-/-}$ mice, treated or untreated, compared to $Agl^{+/+}$ mice (**Supplementary Figure 6A**), suggesting the absence of a mechanism compensating the increased glycogen accumulation with an enhancement of the lysosomal degradation pathway. In addition, as observed in the previous protocol, p62 protein levels were similar between $Agl^{+/+}$ and $Agl^{-/-}$ mice and were not increased by rapamycin treatment after 2.5 months of wash-out of the drug (**Supplementary Figure 6B**). Interestingly, P-Gys1/Gys1 proteins ratio, elevated in $Agl^{-/-}$ mice, was rescued only when rapamycin and AAV9-LiMP-GDEov were used in combination (**Supplementary Figure 6C**), confirming the necessity to combine the expression of GDE and Rapamycin to fully rescue the glycogen metabolism in skeletal muscles of $Agl^{-/-}$ mice. These data support our current working hypothesis that in skeletal muscle, the transient effect of rapamycin on autophagy induction is beneficial only when combined with the clearance of cytosolic glycogen by re-expression of GDE.

Taken together, the biochemical and functional data and the extended bioinformatic analyses suggest that while gene therapy treatment alone rescues the metabolic impairment in GSDIII mice, autophagy induction by rapamycin simultaneous to GDE transgene expression by AAV gene therapy are both contributing to achieve a significant correction of the muscle phenotype in GSDIII mice.

AAV9-LiMP-GDEov has an immunological footprint in GSDIII liver reverted by rapamycin treatment.

To evaluate the molecular events underlying the phenotypical correction observed after AAV9-LiMP-GDEov treatment in the liver, we performed an RNA-seq analysis to compare the transcriptomic changes occurring in AAV-treated $Agl^{-/-}$ animals.

Principal component analysis (PCA) performed on all the genes showed that the largest principal component (PC1) supported a clear separation between PBS-treated $Agl^{-/-}$ and $Agl^{+/+}$ mice (**Figure 7A)**. Interestingly, AAV9-LiMP-GDEov-treated $Agl^{-/-}$ mice, that were equidistant from $Agl^{-/-}$ and $Agl^{+/+}$ mice in PC1, were completely separated from the untreated groups in the second principal component (PC2) (**Figure 7A**).

To further decipher the effect of the AAV vector treatment, differential expression analysis was performed among the four groups. In the liver, 139 DEGs were reported among all conditions, with only 30 genes (21 upregulated and 9 downregulated) being dysregulated between $Agl^{+/+}$ and $Agl^{-/-}$ mice (**Figure 7B,C** and **Supplementary Table 7**). Interestingly, the highest number of DEGs, 97 (76 gene up-regulated and 21 down-regulated), was observed between PBS and AAV9-LiMP-GDEov-treated $Agl^{-/-}$ mice, while more than two times less DEGs, 41 (18 genes up-regulated and 23 down-regulated), were identified in $Agl^{-/-}$ mice treated with the combination of AAV9-LiMP-GDEov with rapamycin as compared to control animals (**Figure 7B,C** and **Supplementary Table 7**).

A heatmap was constructed to visualize similarities and differences in gene expression profiles of DEGs (**Figure 7D**). As predicted by the PCA analysis, AAV9-LiMP-GDEov-treated $Agl^{-/-}$ mice had a distinctive gene expression pattern although most of the genes up-regulated in $Agl^{-/-}$ mice treated with AAV9-LiMP-GDEov were not dysregulated when mice received the combination of AAV9-LiMP-GDEov with rapamycin.

Taken together, these data suggest that the expression of GDE by AAV changes the transcriptional profile of $Agl^{-/-}$ mice without reverting them to $Agl^{+/+}$ mice. Rapamycin treatment seems to somehow antagonize this effect leading to a partial normalization of the AAV treated livers.

To further characterize the specific effect induced by AAV9-LiMP-GDEov in the liver, a Gene Ontology (GO) analysis was then performed on the DEGs identified between untreated $Agl^{-/-}$ mice and mice of the same genotype treated with AAV9-LiMP-GDEov alone or in combination with rapamycin (**Figure 7E-G** and **Supplementary Table 8**). Notably, most of the down-regulated DEGs in $Agl^{-/-}$ versus AAV9-

LiMP-GDEov-treated mice were enriched in pathways related to fatty acids, carbohydrates, and glycogen metabolism (**Figure 7E, F** and **Supplementary Table 8**). On the contrary, the up-regulated DEGs in *Agl*^{-/-} versus AAV9-LiMP-GDEov-treated mice had the highest p-value and were enriched in pathways such as response to interferon-beta, negative regulation of viral process, down-regulation of viral life cycle and regulation of innate immune response (**Figure 7E, F** and **Supplementary Table 8**). Among the pathways related to immune response, some were also identified in GSDIII mice treated with AAV9-LiMP-GDEov in combination with rapamycin, although with a lower p-value (**Figure 7G** and **Supplementary Table 8**).

To understand whether the response to AAV in GSDIII mice was dependent on the IFN response genes, we performed an extended analysis on a subset of DEGs involved in the interferon response as identified by the interferome database (39, 40). While no differences were observed between *Agl*^{+/+} and *Agl*^{-/-} mice, we found that 57 out of 63 interferon response genes were increased in GSDIII mice treated with the AAV9-LiMP-GDEov vector as compared to PBS-treated *Agl*^{-/-} mice (**Supplementary Figure 7**). Of note, treatment with rapamycin reduced the level of expression of 55 genes (**Supplementary Figure 7**) thus supporting the involvement of this pathway in the immune footprint of AAV vectors observed in GSDIII mice and counteracted by rapamycin treatment.

Further characterization of the cells infiltrating the liver was performed by immunofluorescent staining of CD8+ cells and *CD8* mRNA expression level. No significant differences were observed in the level of infiltrates measured in mice injected with AAV9-LiMP-GDEov vector as compared to PBS-treated control mice suggesting a limited effect on the infiltrating CD8+ T cells 2.5 months after the rapamycin treatment (**Supplementary Figure 8A,B**).

These results suggest that while significant transcriptional changes occurred after treatment with AAV9-LiMP-GDEov in GSDIII livers, at 2.5 months after rapamycin treatment there was no evident effect on the number of infiltrating CD8+ cells. To evaluate any contribution of the GSDIII background on the activation of the immune response, we performed a characterization of the immune cells

infiltrating the liver in 6-month-old $Agl^{+/+}$ and $Agl^{-/-}$ mice (**Supplementary Figure 8C**). An increased number of infiltrating immune cells in $Agl^{-/-}$ mice was observed as measured by counting the total CD45+ cells (**Supplementary Table 9**). While no differences were observed in the number of neutrophils or T lymphocytes populating the livers of GSDIII mice, a significant increase was observed in CD11b+ F4/80+ liver macrophages (**Supplementary Table 9**). When activation markers were evaluated, both M1 and M2 polarized macrophages (expressing CD80 and CD206, respectively) were found to be increased in $Agl^{-/-}$ mice. Interestingly when those numbers were reported as percentage of macrophages, an inverse tendency was observed for the two populations with M1 frequency increased and M2 decreased in $Agl^{-/-}$ mice as compared to $Agl^{+/+}$ (**Supplementary Figure 8D**). Taken together, these data suggest that the GSDIII liver contains a higher number of macrophages with a higher frequency of pro-inflammatory M1 macrophages.

DISCUSSION

Despite the first reports by Illingworth and Cori more than 60 years ago (41), no curative treatment exists for GSDIII. Among the possible causes of this delay, one of the most important is the multi-organ phenotype of GSDIII, with metabolic impairment and muscle weakness as the two main disease manifestations.

Given their capacity to efficiently target several tissues, AAV-base gene transfer appears as an ideal therapeutic option for GSDIII. However, the need to target simultaneously liver and muscle, the high doses needed to treat the muscle and the size of the transgene represent a large barrier toward the development of an effective gene replacement strategy for this disease.

We previously reported dual overlapping AAV vectors to produce full-length GDE after recombination (22). However, the only dual approach able to correct both liver and muscles at short term was the one using a CAG promoter, which may represent a risk regarding immune responses (13, 27, 28) and tumor development in liver (29).

Because of these challenges, we thought to combine the overlapping strategy to express the full GDE transgene with a tandem promoter previously described for efficient liver and muscle targeting (13) and to evaluate the efficacy of such approach at long-term. Importantly, while we observed stability in the correction of muscle phenotype, the metabolic impairment was only transiently corrected possibly because of hepatocytes increased proliferation underlying the hepatic pathology in GSDIII (3, 42).

In an attempt to improve AAV gene transfer efficacy, we focused our attention on the combination of the dual vector approach with rapamycin. Rapamycin, an FDA-approved drug, presents several interesting features for GSDIII treatment. First, the use of this drug has been reported to reduce glycogen accumulation and prevent fibrosis in a dog model of GSDIII (26). Second, rapamycin is an autophagy-inducer, and autophagy has been reported to be impaired in muscle of GSDIII patients (31). Finally, rapamycin is widely used in the clinic as an immunosuppressive drug and demonstrated the capacity to delay the immune response after AAV vector administration (32, 43-45) and to increase AAV transduction in the liver, in mouse and in NHP (36, 37, 46).

Surprisingly, in GSDIII mice, rapamycin treatment alone had no effect on glycogen accumulation possibly due to differences in the dose of rapamycin used in GSDIII dogs and the duration of the treatment (26). Interestingly, the levels of p62, a protein that accumulates in autophagosomes, already increased in the liver of GSDIII mice were only slightly reduced by rapamycin treatment suggesting an underlying block of autophagy in this tissue. On the contrary, p62 levels were unchanged in GSDIII muscle and when autophagy was induced by rapamycin treatment, we observed an accumulation of this autophagosome marker suggesting an impairment in the clearance of autophagosomes. Although these data may seem counterintuitive, our working hypothesis is that the slower clearance rate of autophagosomes may be due to the glycogen overload of autophagosomes that saturates the GAA activity in GSDIII muscle.

Given this difference in the autophagy activation observed in the two tissues, we hypothesized that autophagy induction by rapamycin treatment combined with glycogen clearance by the re-expression of the GDE transgene may synergize, in particular in the muscle where the autophagy induction seems limited by the extensive glycogen accumulation.

Differently from what previously reported (36-38), rapamycin treatment in liver did not result in increased transduction and it seems to induce some degree of toxicity. We consider that this may be due to differences in the drug used, i.e. encapsulated vs. free rapamycin, the time of treatment and the doses used. However, one intriguing hypothesis may be that the difference observed might be due to the abnormal autophagic flux observed in GSDIII mice and the absence of autophagy induction.

AAV9-LiMP-GDEov treatment either alone or in combination with rapamycin was able to rescue the metabolic impairment and glycogen accumulation in liver and heart. Importantly, GSDIII mice treated with the combination of AAV9-LiMP-GDEov and rapamycin showed better rescue of glycogen accumulation and muscle strength than those treated with the vector alone, suggesting that the hypothesized synergism was indeed present at least in this tissue. The synergic effect was also evident at the molecular level when an RNAseq analysis was performed in triceps. In particular, the lysosomal pathway was impaired in the muscle of untreated GSDIII mice, thus providing a potential rationale on the lack of efficacy when autophagy was induced by rapamycin. It is thus conceivable to hypothesize that the cytosolic glycogen clearance achieved by gene replacement with GDE facilitates autophagy induction by rapamycin ultimately leading to a complete normalization of the lysosomal pathway and a full restoration of the glycogen degradation pathway in muscle fibers.

To evaluate whether rapamycin treatment had a similar effect on the liver, we performed a transcriptomic analysis in liver. Surprisingly we identified a clear gene expression pattern in $Agl^{-/-}$ mice treated with the vector. Functional analysis of the genes modified by the AAV9-LiMP-GDEov treatment revealed that almost all of them were interferon-responsive genes. Immunosuppressive rapamycin treatment performed at the time of the injection was able to decrease the activation of these genes

thus suggesting a role of the immune system in the early responses to AAV vectors in the liver of GSDIII mice.

These findings indicate that, in GSDIII mice, expression of the GDE transgene results in the formation of low-level anti-GDE antibodies as well as in a tendency toward increased infiltration of CD8+ cells in the liver. The presence of CD8+ cells in the liver could be related to the establishment of a tolerance status toward the transgene (47, 48) that was not rejected in muscle in the long-term experiment presented in this manuscript. One captivating finding of this manuscript is the reported presence of a larger population of macrophages M1 and M2 in the GSDIII liver at the time of vector injection. M1 macrophages play a proinflammatory role, while M2 macrophages are generally anti-inflammatory, promote immunomodulation and are involved in tissue reparation. When the frequency of these macrophage population was measured relative to the total infiltrating macrophages, we found a tendential increase in M1 and a decrease in M2 macrophage populations suggestive of a pro-inflammatory environment in the GSDIII liver. Interestingly, rapamycin treatment has been reported to polarize macrophage differentiation toward an M2 phenotype (49). Here, we hypothesize that the reduction of the immune footprint of the AAV vector measured 2.5 months after the wash-out of rapamycin may be due to an M2 polarization promoted by the drug that resulted in a better control of the immune response toward the AAV vector. Further evaluation of the determinants of the immune response in GSDIII mice and in particular of the role of non-parenchymal cell profile in the formation of the immune response and the persistence of the GDE transgene is currently ongoing.

One limitation of our study is the use of only one dose, one duration and one route of administration of rapamycin. Testing multiple doses of rapamycin in particular could be of interest in this disease, as rapamycin effect is known to be different according to the dose (50). Further investigations of the detailed mechanism behind this immune response to the vector are ongoing although we consider the pre-fibrotic status of the liver as an important component of this response.

One important conclusion of this study is that the combination of rapamycin and gene therapy could potentially reduce the dose of AAV required for the treatment of GSDIII. However, in our study, the total dose of AAV used is about 6×10^{13} vg/kg (3×10^{13} vg/kg of each AAV), not far from doses that showed toxicity in the clinic (51, 52). To circumvent the limitation imposed by the use of high doses of AAV vectors, novel approaches based on the use of single AAV vectors expressing a truncated GDE combined with AAV vectors with improved muscle targeting are being evaluated in glycogenosis (53, 54). Regardless, this manuscript provides support to the use of rapamycin in combination with gene therapy and identifies a potential mechanism behind the observed synergism between the small molecule and AAV gene transfer. In the next future, the combination of small molecules with improved AAV gene therapy approaches may increase safety while reducing the effective dose.

Future clinical development of the combination treatment may require optimization of the approach by testing several doses of rapamycin and protocol designs as well as AAV vectors to express GDE in both tissues.

To conclude, these results suggest that GSDIII liver is prone to the development of immune responses to AAV vectors that can be controlled by a transient immunosuppressive treatment and support the development of combination approaches for the treatment of diseases with underlying liver degeneration.

MATERIALS AND METHODS

Clonings and AAV vector production. LiMP promoter was already described(13). Briefly, it consists of the association of the human alpha-1 anti-trypsin and the synthetic spC5-12 promoters. The design of the overlapping vectors was already described (22). The "Head" vector containing the first part of the final sequence is 4.4 kb, and the "Tail" vector containing the end of the final sequence is 4.1 kb. The two overlapping expression cassettes were flanked by the inverted terminal repeats of AAV serotype 2 for vector packaging. Transgene expression cassettes of similar size are fully encapsidated with percentages of full capsids ranging from 30-70% depending on the composition.

AAV vectors were produced by an adenovirus-free transient transfection method(55), and purified as described earlier (56). AAV vector titers were determined by quantitative real-time PCR (qPCR) as already described (22).

Mouse model. All studies were conducted in *Agl* knockout mice (*Agl*$^{-/-}$) and wild-type (*Agl*$^{+/+}$) littermates. Mice generation and phenotype were reported in previous work (22). Briefly, mice were generated in a pure C57BL/6J background by replacing exons 6–10 of the *Agl* gene with a neomycin-expressing cassette, and then bred into a mixed BALB/c background.

Sex as a biological variable. Only males were used in these studies, based on previous reports that AAV liver transduction is less efficient in females than in males (57).

In vivo **studies in mice.** In all mouse studies, animals were randomly assigned to treatment groups. To minimize potential bias during functional assessments in mice, operators were blinded to the study design. Operators in charge of sample analysis were also blinded to study design.

First study: 12 months follow-up after AAV injection. Three-month-old *Agl*$^{-/-}$ mice were injected intravenously with 6 x 10^{13} vg/kg (3 x 10^{13} vg of the 'Head' vector, and 3 x 10^{13} vg of the 'Tail' vector) of AAV9-LiMP-GDE overlapping vector (n=4), or PBS in the controls *Agl*$^{+/+}$ (n=5) and *Agl*$^{-/-}$ (n=4) groups.

Second study: 1-month daily treatment with rapamycin. Rapamycin was injected intraperitoneally to *Agl$^{+/+}$* (n=5) and *Agl$^{-/-}$* (n=6) at a dose of 1.5 mg/kg every day for one month. Controls mice, *Agl$^{+/+}$* (n=5) and *Agl$^{-/-}$* (n=6), were injected with vehicle (NaCl) following the same scheme.

Third study: combination treatment. Six-month-old *Agl$^{+/+}$* and *Agl$^{-/-}$* mice were injected daily intraperitoneally with 1.5 mg/kg rapamycin or vehicle (4 groups: *Agl$^{+/+}$*, rapamycin (n=5) ; *Agl$^{+/+}$*, vehicle (n=5) ; *Agl$^{-/}$*, rapamycin (n=7) ; and *Agl$^{-/-}$*, vehicle (n=9)). After a month, half of the *Agl$^{-/-}$* mice treated with vehicle were injected intravenously with 6 x 10^{13} vg/kg of AAV9-LiMP-GDE overlapping vector (n=5), or PBS (n=4); and half of the *Agl$^{-/-}$* mice treated with rapamycin were injected intravenously with 6 x 10^{13} vg/kg of AAV9-LiMP-GDE overlapping vector (n=4), or PBS (n=3). Rapamycin daily injections were pursued for 15 additional days in these two last groups as well as in the *Agl$^{+/+}$*, rapamycin group. Mice were euthanized 3 months after vector injection (or 2.5 months after the end of the rapamycin treatment) at the age of 9 months.

Wire hang test. Forelimb wire hang test was performed as already reported (22). A 4-mm-thick wire was used to record the number of falls over a period of 3 min. The average number of falls per minute was reported for each animal.

Blood collection, glycemia measures. Normally fed mice were anesthetized for glycemia measurement and blood collection. Blood glucose was measured with an Accu-Check Go glucometer (Roche Diagnostic, Meylan, France) using a drop of blood from retro-orbital sinuses. Then, blood samples were collected by retro-orbital sampling into heparinized capillary tubes and mixed with 3.8% sodium citrate, followed by plasma isolation.

Anti-capsids and anti-transgene responses measurement. First, mice sera were decomplemented by incubating them 30 minutes at 56°C. Then, the concentration of IgM and IgG antibodies was determined by enzyme linked immunosorbent assay (ELISA), as previously described for anti-capsids IgM and IgG(18, 58)**,** and as following for anti-GDE IgG: 96-wells plates were coated with GDE protein (OriGene, Rockville, MD, USA) at 1 µg/ml and incubated overnight at 4°C; wells were saturated with

PBS 6% non-fat milk for 2h at room temperature, and then incubated with decomplemented sera for 1h at 37°C. A biological known positive control, consisting of the decomplemented sera of Sprague-Dawley rats immunized through intramuscular injection of an AAV1 dual vector expressing GDE, was included. A commercial polyclonal rabbit anti-hGDE (16582-1-AP, ProteinTech, Rosemont, IL, USA) diluted at 1:1000 was used as an internal control for coating. Secondary sheep anti-mouse IgG-HRP (GE healthcare, Chicago, IL, USA) and goat anti-rat IgG-HRP antibodies (ThermoFisher Scientific, Waltham, MA, USA) were diluted at 1:5000, while secondary goat anti-rabbit IgG-HRP antibody (Agilent DAKO, Santa Clara, CA, USA)was diluted at 1:2000, and then incubated 1h at 37°C. 3,3',5,5'-tétraméthylbenzidine substrate (TMB) (BD Biosciences, San Diego, CA, USA) was incubated 15 minutes at room temperature for revelation, then the reaction was stopped using H_2SO_4 2N before reading the absorbance at 450 nm and 570 nm (for back-ground subtraction) on an EnSpire alpha plate reader (PerkinElmer, Waltham, MA, USA).

Western Blot analysis. Snap-frozen tissues were homogenized in UltraPure DNase/RNase-free water (Thermo Fisher Scientific, Waltham, MA) in the first study, or in RIPA buffer (R0278, Sigma-Aldrich) mixed with Complete™ protease-inhibtor cocktail (11697498001, Sigma-Aldrich) in the second and the third studies, with FastPrep lysis tubes (MP Biomedicals, Ohio, USA), followed by centrifugation 20 min at 10,000×g to collect the supernatant. Protein content in lysates was quantified by BCA Protein Assay (Thermo Fisher Scientific, Waltham, MA). SDS-page electrophoresis was performed with NuPAGE 4–12 % Bis-Tris protein gels (Life technologies, Carlsbad, CA). After transfer, the membrane was blocked with Odyssey buffer (LI-COR Biosciences) and incubated with an anti-hGDE antibody (rabbit polyclonal, AS09-454, Agrisera in liver, or rabbit polyclonal, 16582-1-AP, Proteintech in muscles), anti-p62/SQSTM1 (ab56416, Abcam), anti-phosphorylated GYS (#3891, Cell signaling), anti-GYS1 (#3886, Cell signaling), anti-vinculin (mouse monoclonal, clone V9131, Sigma-Aldrich), or anti-actin antibody (rabbit monoclonal, sc-8432, Santa Cruz Biotechnology). Membranes were then washed and incubated with the appropriate secondary antibody (LI-COR Biosciences) and visualized with the Odyssey imaging system (Li-Cor Biosciences). Densitometry analysis was conducted using Image Studio Lite (Li-Cor

Biosciences) version 5.2. Protein level was normalized to the housekeeping protein (vinculin or actin) and then to the *Agl*^{+/+} mice.

Measurement of glycogen content. Glycogen content was measured indirectly in tissue homogenates as previously described (22).

Measurement of acid alpha-glucosidase activity. GAA activity was measured in tissue homogenates as previously described [18].

Vector genome copy number. Vector genome copies in mice were determined by qPCR on tissue DNA. Total DNA was extracted from tissues homogenates using the "DNA & RNA isolation Kit from pathogen" (Macherey-Nagel, Hoerdt, France) and the KingFisher apparatus (ThermoFisher) extraction method according to manufacturer's instructions. The primers used in the reaction were located in the human alpha-1 anti-trypsin promoter region (forward primer 5'-GGCGGGCGACTCAGATC-3', reverse primer 5'-GGGAGGCTGCTGGTGAATATT-3'), for the vector. The number of vector copies was normalized by the copies of the *titin* gene, which was used as an internal control for each sample (forward primer: 5'-AAAACGAGCAGTGACGTGAGC-3', reverse primer: 5'-TTCAGTCATGCTGCTAGCGC-3'). Data were expressed as vector genome copies per diploid genome.

Histology and stainings. Immediately after euthanasia, muscles and a piece of liver were snap-frozen in isopentane (-160°C) previously chilled in liquid nitrogen, and a piece of fresh liver was fixed in formaldehyde and embedded in paraffin. Serial cross-sections (8 mm for muscles and 4 mm for liver) were cut in a Leica CM3050 S cryostat (Leica Biosystems, Wetzlar, Germany). To minimize sampling error, 2 or 3 sections of each specimen were obtained and stained with haematoxylin and eosin (HE) or with periodic acid-Schiff (PAS), and red Sirius (RS) for liver, according to standard procedures. Images were acquired using an Axioscan slide scanner (ZEISS, Munich, Germany), using a plan-apochromat 10 x magnitude 0.45 NA objective. Tile scan images were reconstructed with ZEN software (ZEISS, Germany). Anti-CD8 immunostaining was performed according to standard procedures on frozen serial liver slices at a dilution of 1:40, using a monoclonal anti-CD8α antibody (monoclonal rat antibody, clone

CT-CD8a, Invitrogen, Ref: MA5-17594). For CD8+ cells quantification, images were processed using QuPath 0.4.3 Software. A first pixel classifier was trained on different types of liver slices for detecting tissue and eliminating artefacts such as folding, bubbles and tearings. This contour pixel classifier is a Random Tree with a resolution of 5.2µm/pixel, includes 2 channels, 3 scales (2,4, 8), 5 features (Gaussian, Laplacian of Gaussian, Weighted Deviation, Gradient Magnitude and Structure Tensor Max Eigenvalues) and no local normalization. The quantification of CD8+ cells was performed using the included Cell Detection feature on the fluorescence channel of the CD8 staining, using the following parameters: Pixel size 1µm, Background radius 10µM, median filter radius 1.5µm, Sigma 2µm, minimum and maximum area respectively 30 and 400µm², the threshold was set to 1600 and the cell expansion set to 0µm. The resulting detections are the CD8+ cells.

The output parameter is the ratio of the number of CD8 positive cells over the total surface area of the tissue slice, expressed as cells per millimeter square. The quantification of CD8+ cells was performed using a pixel classifier trained on healthy tissue and impaired tissue. The output parameter is the ratio of the number of CD8 positive cells over the total number of cells on the total tissue slice (quantified by DAPI positive staining).

RNA extraction. Tissues were lysed with FastPrep lysis tubes (MP Biomedicals, Ohio, USA) using Qiazol (Qiagen, Venlo, The Netherlands) and chloroform (Sigma-Aldrich, MI, USA) reagents. RNA was isolated using RNeasy Plus Mini extraction kit (Qiagen, Germany) according to the manufacturer's instructions. DNase I digestion (Invitrogen, USA) was performed to degrade DNA in the sample. Quantification and quality control of RNA samples were determined using Agilent RNA ScreenTape System (5067-5576, Agilent, Santa Clara, CA, USA) following manufacturer's instructions.

RNA sequencing and transcriptomic analysis. For each sample, 100 ng of total RNA was used to perform the QuantSeq 3' mRNA-Seq Library Prep FWD for Illumina (Lexogene, Vienna, Austria) resulting in NGS libraries which originate from the 3' end of polyadenylated RNA. Briefly, library generation was started by oligo(dT) priming with primers. After first strand synthesis, the RNA was

removed before the second strand synthesis was initiated by random primers. Libraries were PCR amplified and barcoded in 17 cycles and were quantified using Agilent High Sensitivity DNA kit (Agilent). 2nM of pooled libraries were denatured and 1.8pM was used for cluster generation before single-end sequencing on an Illumina Nextseq550 (Illumina, US, High output 2*75pb run). Samples were sequenced with an average of 13,232,481 reads per sample. The quality control of the sequencing data was evaluated using FastQC (v0.11.9). The reads were trimmed using Prinseq-lite v0.20.4(59) (--trim-right 20) and filtered by average quality score (--trim-qual 20) and cutadapt v1.18. Reads were mapped on EnsEMBL GRCm38.99 mouse reference using rna-STAR v2.7.6a(60). Reads below a mapping score of 10 or multimapped were filtered using samtools v0.1.18(61). The gene expression level in each sample was quantified with HTSeq-count v0.12.4(62). The differential gene expression (DEG) between conditions was calculated with DESeq2 v1.34.0(63) using R v4.1.2). We consider that genes are differentially expressed when their BaseMean is greater than 20, their Benjamini and Hochberg adjusted p-value adjusted is less than 0.05 and |log2FoldChange| is upper than 0.4 (options: lfcThreshold = 0.4, altHypothesis = 'greaterAbs'). Data are available on the GEO database (GSE232166) and programming codes for DEG analysis are available on Github (https://github.com/I-Stem-CECS/NGS79) The heatmap of the differentially expressed genes among all pairwise comparisons untreated $Agl^{+/+}$ and $Agl^{-/-}$, and $Agl^{-/-}$ mice treated with AAV9-LiMP-GDEov alone or AAV9-LiMP-GDEov combined with rapamycin using the ComplexHeatmap package(63). Functional annotation analysis of differentially expressed genes and Gene Set Enrichment Analysis (GSEA) (64) were performed using cluster Profiler package (65) in R. Gene Ontology (GO) terms (66) and KEGG pathways (67) were retrieved from the analysis. Enrichments were considered significant if associated to an adjusted p-value < 0.05. K-means clustering analysis was performed on a set of genes from the lysosome pathway in KEGG. The 5 clusters identified contained genes with similar expression levels. These clusters have been discriminated into 3 sub-groups: i) unaffected by the disease, modified by the treatment, ii) modified by the disease, not rescued and, iii) modified by the disease, rescued.

Reverse transcription and qPCR. 2μg of RNA were subjected to the "DNA-free kit" (Invitrogen, USA) and to reverse transcription using the "RevertAid First Strand cDNA Synthesis Kit" (ThermoFisher). The cDNA obtained were quantified using TaqMan® mixes for CD8 (Mm01182107_g1) and RPLP0 as housekeeping gene (Mm00725448-s1) (ThermoFisher). Data were expressed as -ΔΔCt which are the Ct normalized with the housekeeping gene values and normalized to AgI$^{+/+}$ group values.

Flow cytometry. Mouse livers were dissociated onto a 70 μm nylon mesh cell strainer in ice cold phosphate buffer saline (PBS) buffer and hepatocytes were eliminated by centrifugation at 30g for 3 minutes. The supernatant was then centrifuged at 300g for 5 minutes and the resulting cell pellet resuspended in Percoll to undergo a leukocyte separation step on a Percoll gradient. After centrifugation at 1300g for 20 minutes without acceleration or brake at room temperature, the leukocyte ring was harvested and washed in buffer solution (PBS, 2 mM EDTA, 0.1% human serum albumin (HSA)). Immunostaining for flow cytometry was performed using standard protocols where non-specific binding of Immunoglobulin to Fc receptors is blocked with anti-mouse FcγRIII/II (clone 2.4G2). Cells were then incubated for 30 minutes in PBS labeling buffer, 2 mM EDTA, 0.1% HSA with LIVE/DEAD™ Fixable near IR Dead Cell Stain (Invitrogen) and antibodies of interest (CD3-Alexa Fluor 488, CD11b-Percp-efluor710, CD80-PE, CD8-PE-Cy7, CD206-APC, Gr1-efluor450, F4/80-Super bright 780, CD45-Brilliant ultra violet 395, CD4-Brilliant ultra violet 496).). Cells were fixed with 4% PFA for 15 minutes. Experimental data was acquired on a CytoFLEX LX flow cytometer (Beckman Coulter®). All labeling and centrifugation steps were carried out at 4°C. VersaComp Antibody Capture Bead Kit (Beckman Coulter®) compensation beads were used to perform the compensations. Obtained data was processed with FlowJo™ v10.7.2 software (Becton, Dickinson and Company©).

Statistical analysis. All data shown in the present manuscript are expressed as mean ± standard deviation (SD). GraphPad Prism 7.0 software (GraphPad Software, San Diego, CA) was used for statistical analyses. p-value < 0.05 was considered significant. Parametric tests were used for data having a normal distribution with α = 0.05. One-way ANOVA with Tukey's post hoc correction was used

for comparisons of one variable between more than two groups. All statistical tests were performed two-sided. The statistical analysis performed for each dataset is indicated in the figure legends.

Study approval. *In vivo* studies were performed in compliance with all relevant ethical regulations for animal testing and research. Notably, they were performed according to the French and European legislation on animal care and experimentation (2010/63/EU) and approved by Genethon's ethical committee.

Data availability. All data presented in the manuscript are either shown in histograms as individual points and/or reported in tables and reported in a separate Supporting data values file. The RNAseq data are available as a Gene Expression Omnibus (GEO) dataset (GSE232166).

Author Contribution. LJ, MV, QM performed or directed experimental activities, contributed significantly to experimental design, data analysis, and manuscript writing. MJ and HP performed the RNA sequencing. LH, XN and GR conceived the study, directed experimental activities and data interpretation, and wrote the manuscript. LR, PV, VMR, HS, JN, PLB, LB, AF, JR, DAG and FC provided insight into the disease pathophysiology, AAV vector technology and immunology. JC developed the

pipeline for the analysis of the liver infiltrates. FB, EBF, CG, LVW, AM and ND contributed to experimental activities. All authors approved the final manuscript.

Conflict of interests. GR and PV are authors in patents related to the development of gene therapy approaches for GSDIII. All other authors declare no conflict of interest.
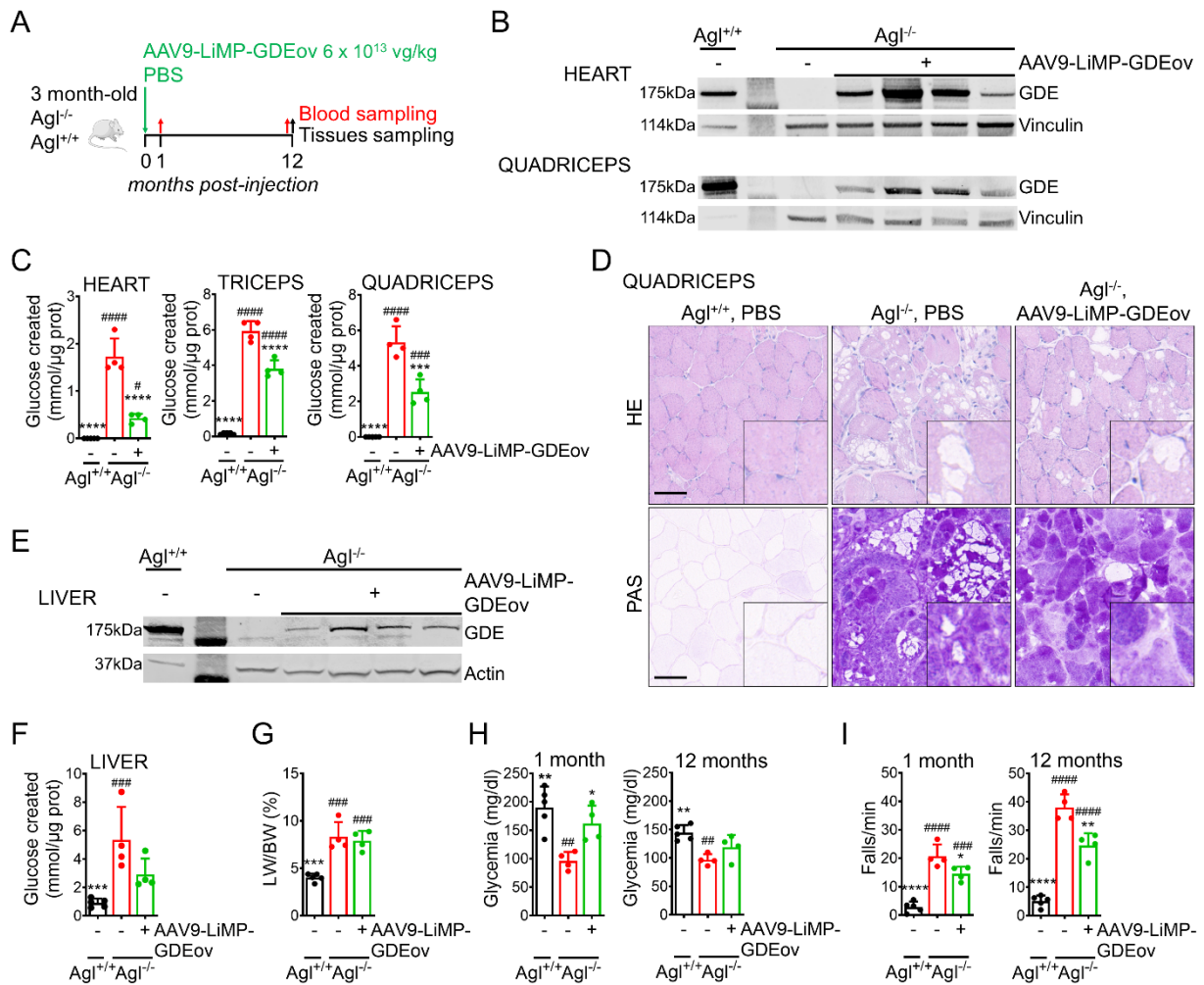
FIGURE 1

Figure 1. AAV9-LiMP-GDEov achieves partial correction of the muscles but correction is lost overtime in liver of *Agl⁻/⁻* mice. A. 3-month-old *Agl⁻/⁻* mice received a single injection of AAV9-LiMP-GDEov at 6x10^{13} vg/kg total (n = 4 per group) and followed-up for 12 months. PBS-injected *Agl⁺/⁺* (n = 5) and *Agl⁻/⁻* (n = 4) mice were used as controls. **B.** Western blot analysis of GDE in heart and quadriceps. **C.** Glycogen content in heart, quadriceps, and triceps 12 months after vector injection. **D.** Hematoxylin and Eosin (HE) and Periodic Acid Schiff (PAS) staining performed in quadriceps sections; scale bar 100 μm. **E.** Western blot analysis of GDE in liver. **F.** Glycogen content in liver 12 months after vector injection. **G.** Liver weight expressed as a percentage of body weight measured 12 months after vector injection. **H.** Glycemia measured one month or twelve months after vector injection. **I.** Wire hang test shown as number of falls per minute performed one month or twelve months after vector injection. Data are shown as mean ± SD. Statistical analyses were performed by one-way ANOVA with Tuckey

post-hoc test. Significance was indicated with * vs. $Agl^{-/-}$ and # vs. $Agl^{+/+}$. * and # $p<0.05$, ** and ## $p<0.01$, *** and ### $p<0.001$, **** and #### $p<0.0001$.
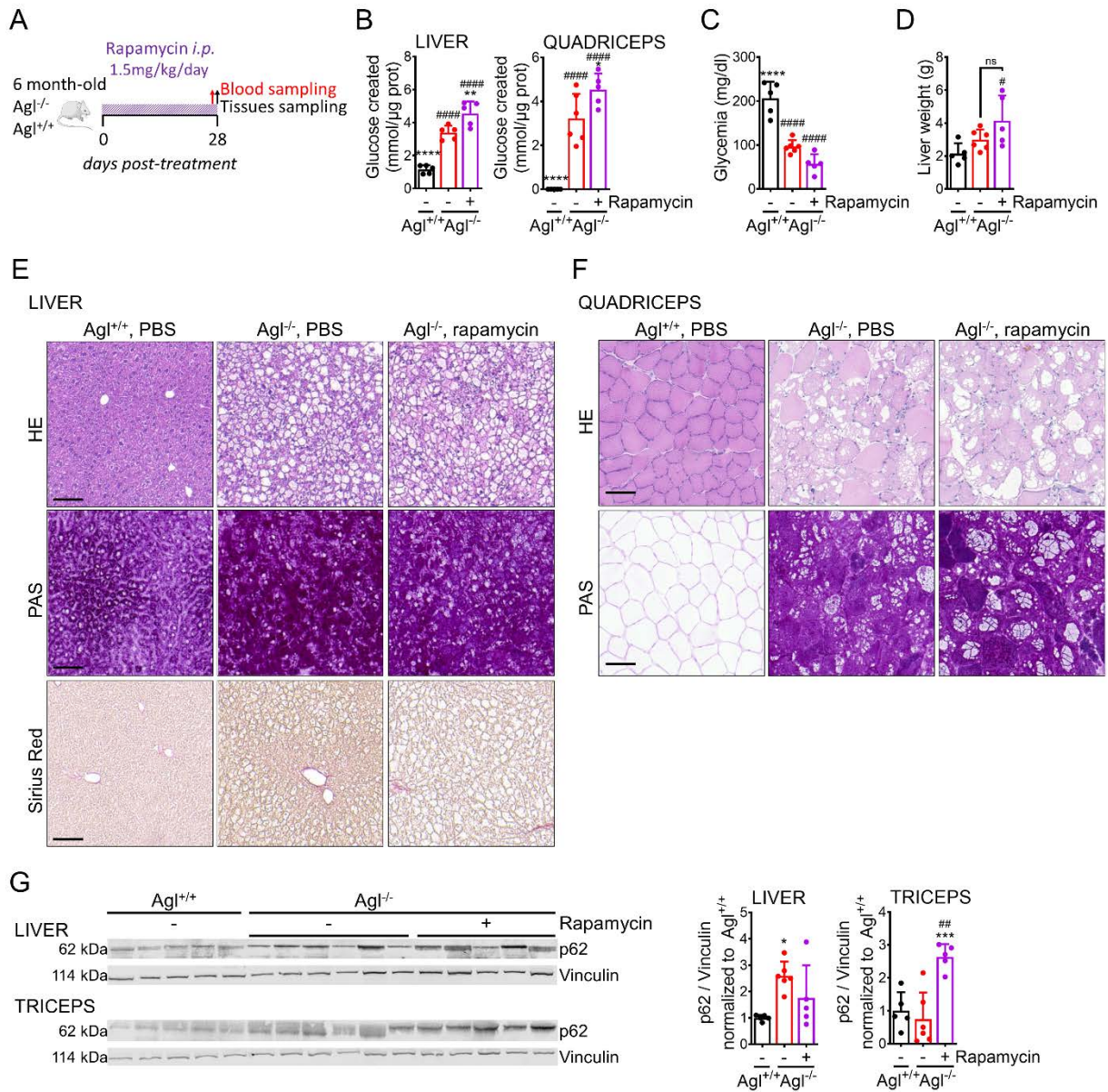
FIGURE 2

Figure 2. One-month daily rapamycin treatment fails at rescuing liver and muscle impairment in *Agl⁻/⁻* mice. A. 6-month-old *Agl⁻/⁻* mice received daily intraperitoneal injections of rapamycin at 1.5 mg/kg for a month (n = 5 per group). Vehicle-injected *Agl⁺/⁺* (n = 5) and *Agl⁻/⁻* (n = 5) mice were used as controls. **B.** Glycogen content measured in liver and quadriceps at the end of the treatment. **C.** Glycemia measured at the end of the treatment. **D.** Liver weight measured at the end of the treatment. **E**. Hematoxylin and Eosin (HE), Periodic Acid Schiff (PAS), and Sirius red staining performed in liver sections; scale bar 100 μm. **F.** Hematoxylin and Eosin (HE), and Periodic Acid Schiff (PAS) staining performed in quadriceps sections; scale bar 100 μm. **G.** Western blot analysis of p62 in liver and triceps. Quantifications of p62 proteins bands are plotted next to the Western blot and expressed as ratio to vinculin. Data shown as mean ± SD. Statistical analyses were performed by one-way ANOVA with

Tuckey post-hoc test. Significance was indicated with * vs. *Agl*$^{-/-}$ and # vs. *Agl*$^{+/+}$. * and # $p<0.05$, ** and ## $p<0.01$, *** $p<0.001$, ****, and #### $p<0.0001$, ns not significant.
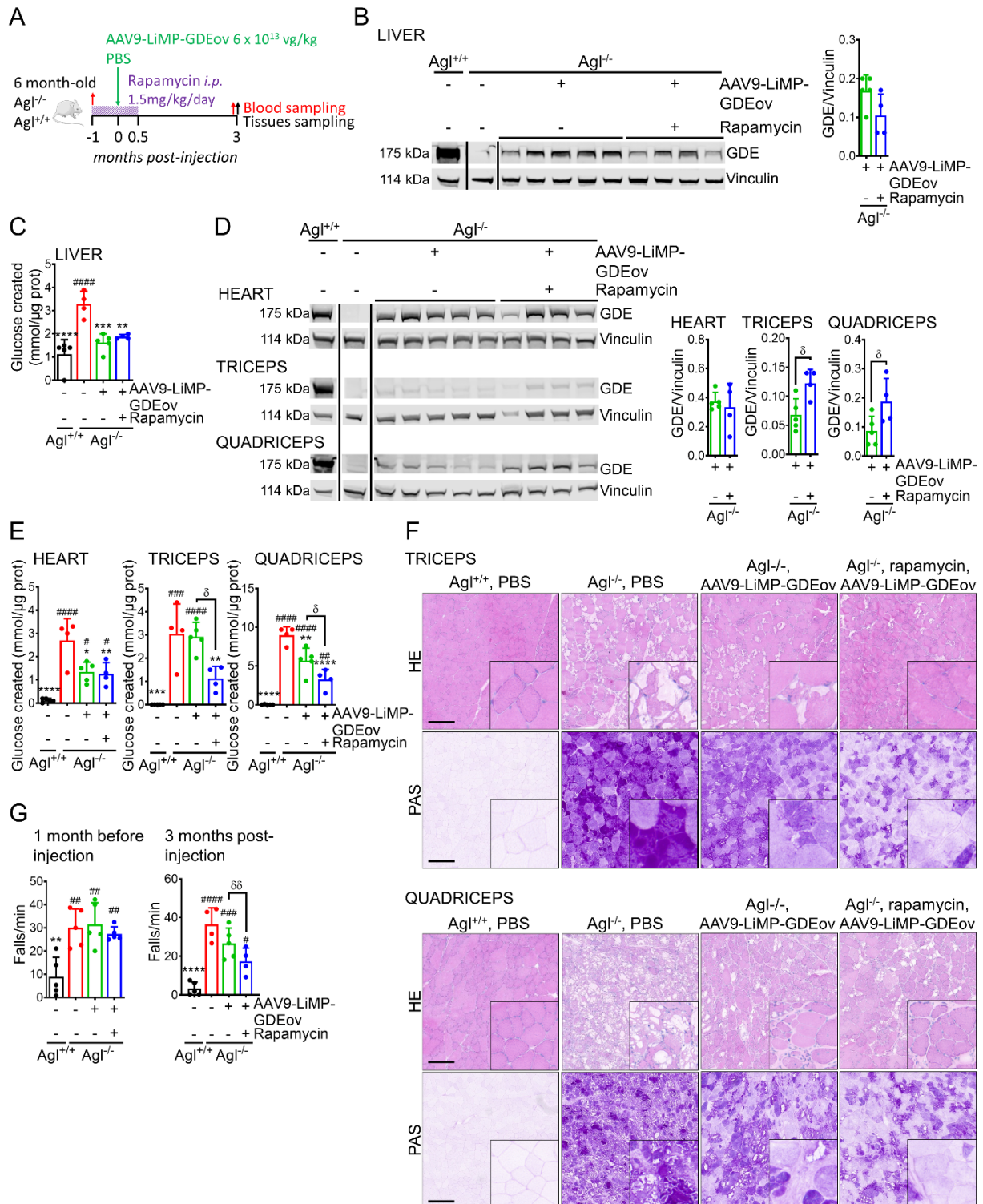
FIGURE 3

Figure 3. Combination of AAV9-LiMP-GDEov and rapamycin corrects the liver and the muscle impairment in symptomatic *Agl⁻/⁻* mice. A. 6-month-old *Agl⁻/⁻* mice received daily intraperitoneal injections of rapamycin at 1.5 mg/kg or vehicle for 6 weeks and were injected with AAV9-LiMP-GDEov at 6 x 10¹³ vg/kg (n = 4 per group) four weeks after the beginning of the rapamycin treatment. Vehicle-

33

injected $Agl^{+/+}$ (n = 5) and $Agl^{-/-}$ (n = 4) mice received daily injection for 6 weeks. **B.** Western blot analysis of GDE in liver. The quantification of the GDE protein bands is plotted on the right expressed as ratio to vinculin. **C.** Glycogen content in liver measured three months after vector injection. **D.** Western blot analysis of GDE in heart, quadriceps, and triceps. The quantification of GDE protein band is plotted on the right expressed as ratio to vinculin. **E.** Glycogen content in heart, quadriceps, and triceps three months after vector injection. **F.** Hematoxylin and Eosin (HE) and Periodic Acid Schiff (PAS) staining performed in triceps and quadriceps; scale bar 200 μm. **G.** Wire hang test shown as number of falls per minute performed one month before the beginning of the rapamycin treatment and three months after vector injection. Data shown as mean ± SD. Statistical analyses were performed by one-way ANOVA with Tuckey post-hoc test. Significance was indicated with * vs. $Agl^{-/-}$ and # vs. $Agl^{+/+}$ or δ as indicated. δ, * and # $p<0.05$, δδ, ** and ## $p<0.01$, *** and ### $p<0.001$, **** and #### $p<0.0001$.
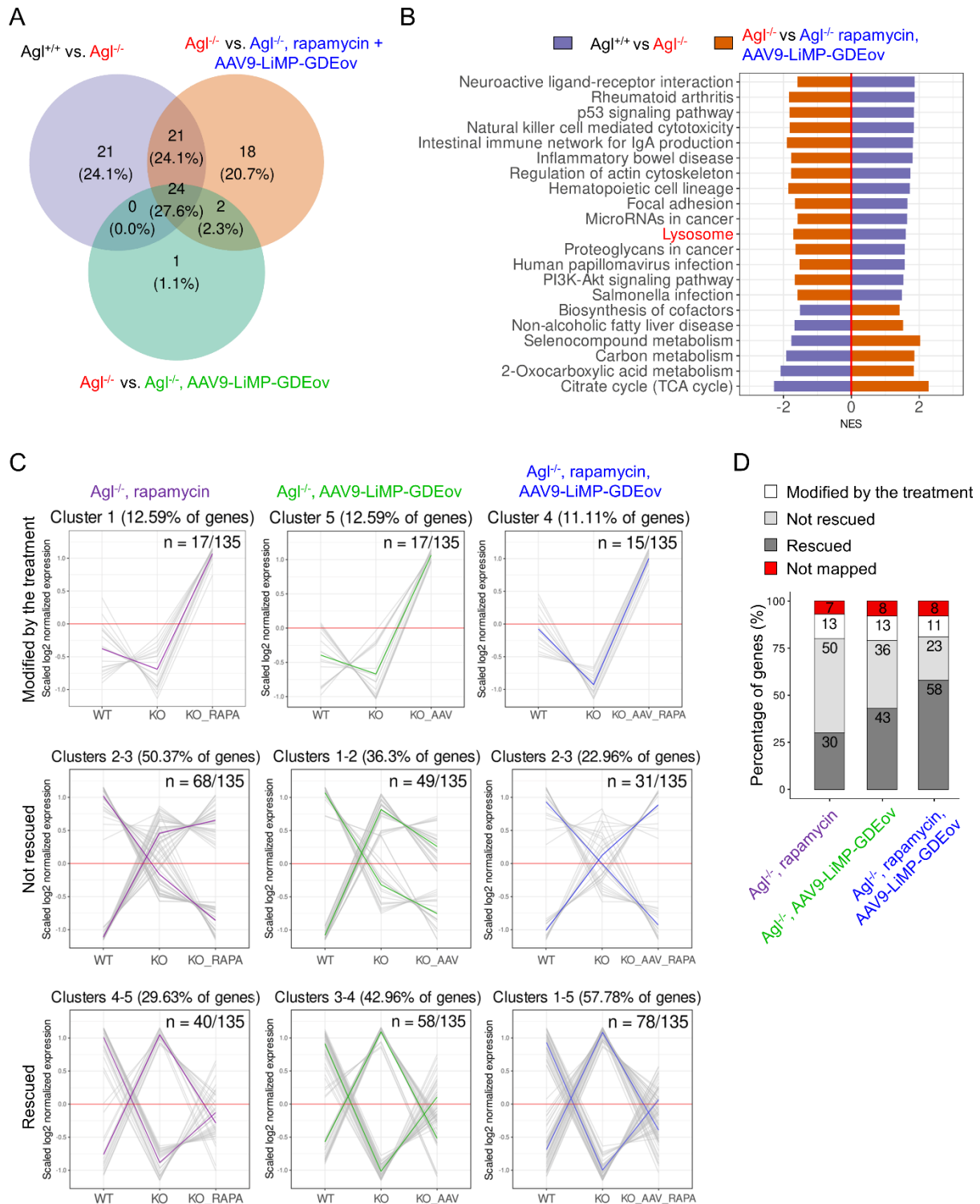
FIGURE 4

Figure 4. RNA-seq analysis supports the synergic effect of AAV9-LiMP-GDEov and rapamycin treatment to correct *Agl⁻ᐟ⁻* mice and rescue the lysosomal pathway impairment in triceps. A. Venn diagram representing the overlap of pathways from Gene Set Enrichment Analysis (GSEA) with KEGG database in *Agl⁺ᐟ⁺ Ag⁻* vs. *Agl⁻ᐟ⁻ ⁺*, *Agl⁻ᐟ⁻* vs. *Agl⁻ᐟ⁻* AAV9-LiMP-GDEov and *Agl⁻ᐟ⁻* vs. *Agl⁻ᐟ⁻* AAV9-LiMP-GDEov,

Rapamycin mice. **B.** Barplot representing the 21 common pathways found dysregulated between $Agl^{+/+}$ vs $Agl^{-/-}$ mice and $Agl^{-/-}$ vs $Agl^{-/-}$ AAV9-LiMP-GDEov, Rapamycin mice by using GSEA with KEGG database. NES, Normalized Enrichment Score. **C.** K-means clustering analysis on the lysosomal pathway genes between the three treatments: $Agl^{-/-}$ mice treated with rapamycin alone, AAV9-LiMP-GDEov alone and the combined treatment. The three clusters identified contained genes in which the expression levels were: i) unaffected by the disease, modified by the treatment, ii) modified by the disease but not rescued by the treatment and, iii) modified by the disease and rescued. Y-axe represents normalized expression counts, averaged for each condition and scaled for each gene. Gray lines represent the expression profile of individual genes. Colored lines represent average expression profiles for each of the clusters. **D.** Comparison of the number of genes in the three sub-families (modified by the treatment, not rescued, rescued) among the three treatments. Values are expressed in percentage of total.
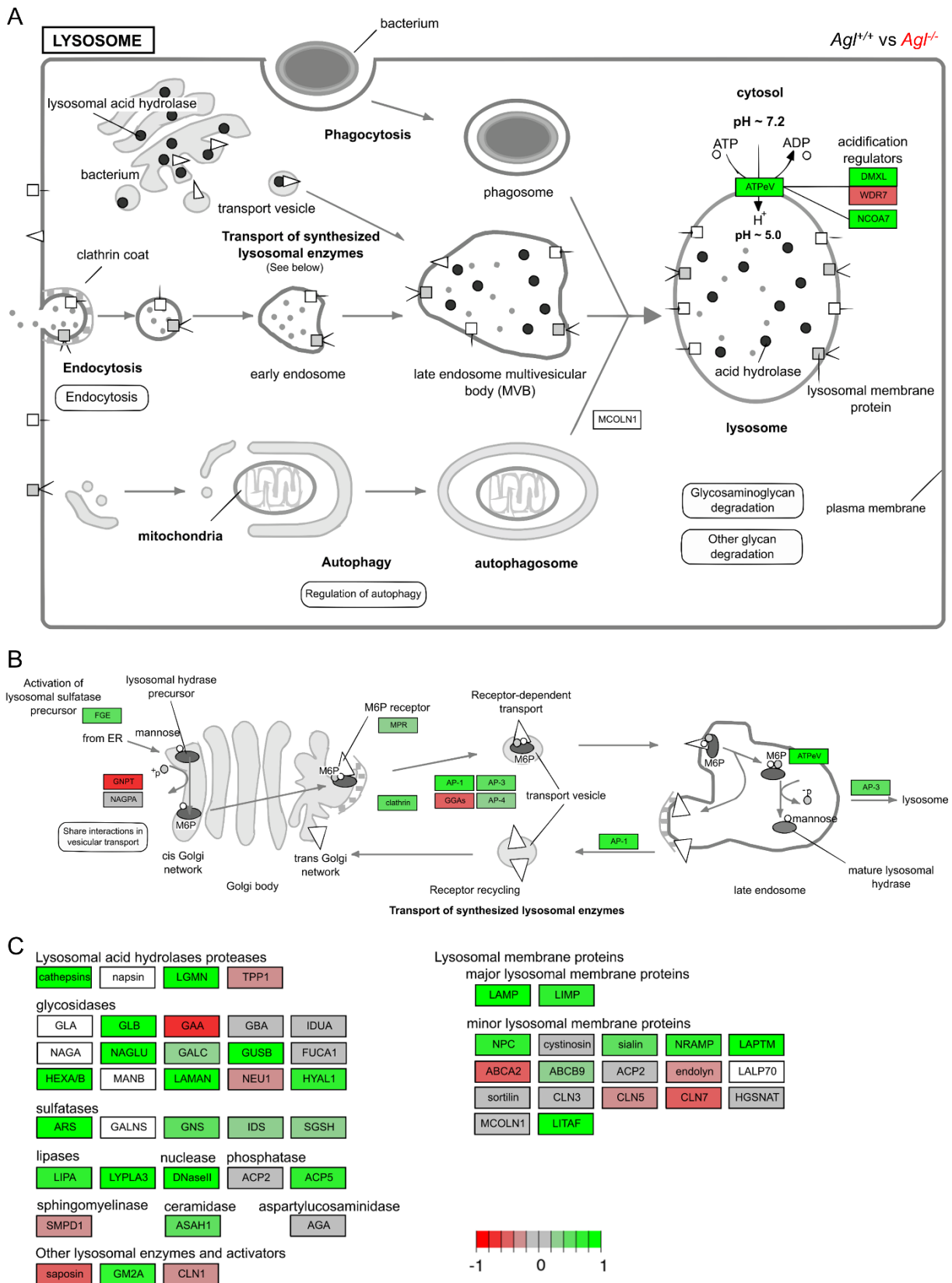
FIGURE 5

Figure 5. Visualization of the lysosome pathway from KEGG (mmu04102) between *Agl*+/+ and *Agl*-/-

mice, in triceps, using Pathview package in R. Proteins and corresponding genes names are indicated

in Supplementary Table 6. Fold-change levels of up-regulated and down-regulated genes are represented in green or red colors, respectively. **A.** Overview of lysosome formation and autophagy. **B.** Transport of newly synthetized lysosomal enzymes to the lysosome. **C.** Main lysosomal proteins and enzymes transcriptomic expression levels.

FIGURE 6

Figure 6. Visualization of the lysosome pathway from KEGG (mmu04102) between *Agl*^{-/-} and *Agl*^{-/-} rapamycin, AAV9-LiMP-GDEov mice, in triceps, using Pathview package in R. Proteins and

corresponding genes names are indicated in Supplementary Table 6. Fold-change levels of up-regulated and down-regulated genes are represented in green or red colors, respectively. **A.** Overview of lysosome formation and autophagy. **B.** Transport of newly synthetized lysosomal enzymes to the lysosome. **C.** Main lysosomal proteins and enzymes transcriptomic expression levels.
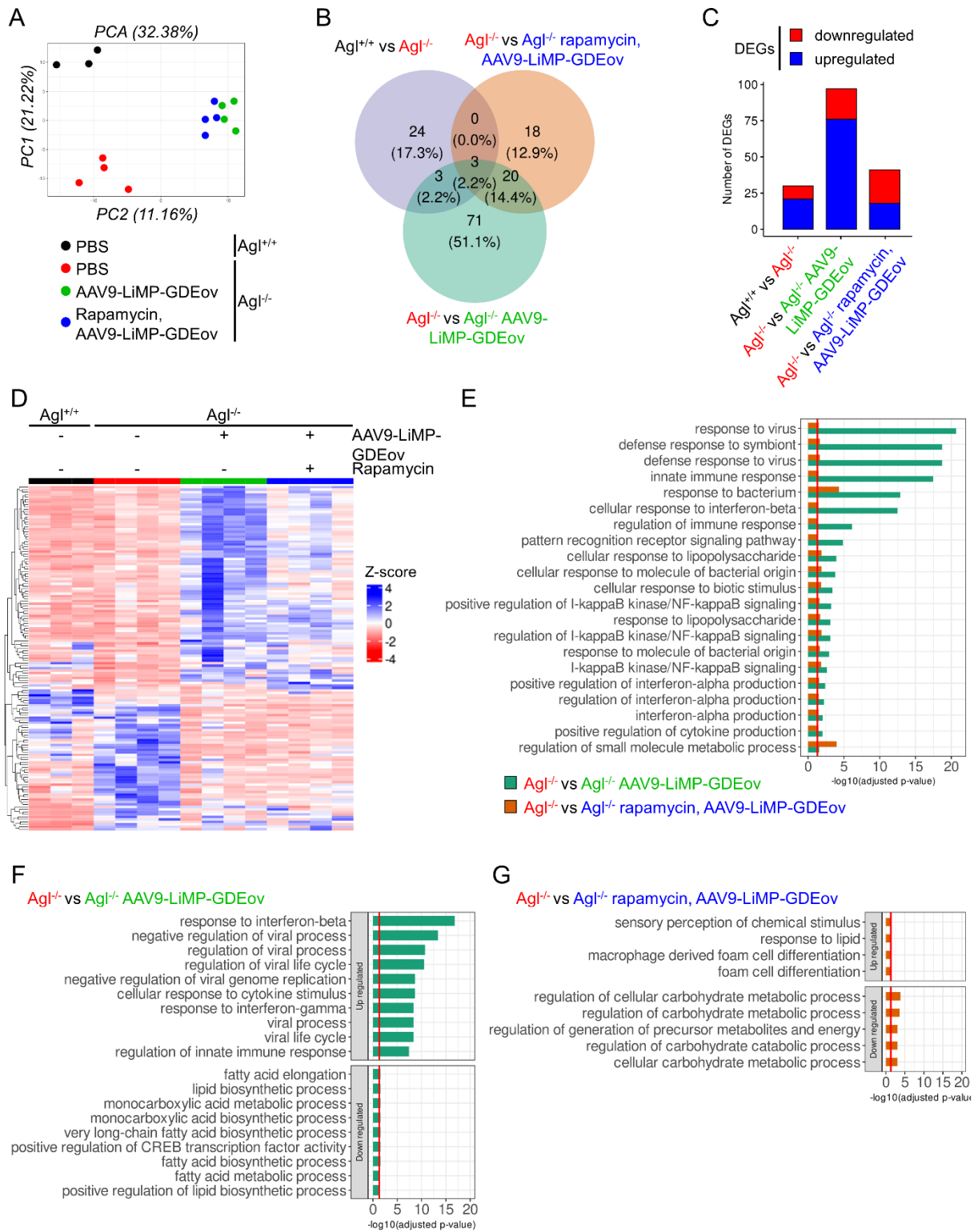
FIGURE 7

Figure 7. RNA-seq analysis reveals an immunogenic footprint induced by AAV9-LiMP-GDEov injection in *Agl⁻/⁻* mice partially reverted by rapamycin treatment in liver. A. Principal Component Analysis (PCA) of RNA-seq data using DESeq2. Samples are colored according to each group. **B.** Venn diagram representing the overlap of DEGs among the three comparisons (*Agl⁻/⁻* vs. *Agl⁺/⁺*, *Agl⁻/⁻* vs. *Agl⁻/⁻* AAV9-

LiMP-GDEov, *Agl*^{-/-} vs. *Agl*^{-/-} AAV9-LiMP-GDEov, Rapamycin). **C.** Number of up and down-regulated genes among differentially expressed genes (DEGs) in each pairwise comparison (*Agl*^{-/-} vs. *Agl*^{+/+}, *Agl*^{-/-} vs. *Agl*^{-/-}, AAV9-LiMP-GDEov, *Agl*^{-/-} vs. *Agl*^{-/-}, AAV9-LiMP-GDEov, Rapamycin). **D.** Heatmap representing the DEGs among all comparisons. Expression levels of up-regulated and down-regulated genes are represented in blue or red colors, respectively. **E.** Barplot depicting the 21 common enriched gene ontology terms (GO) of up and down-regulated DEGs found between *Agl*^{-/-} mice and *Agl*^{-/-} AAV9-LiMP-GDEov-treated mice with and without rapamycin treatment. **F-G.** Barplots showing the top enriched gene ontology terms (GO) of up and down-regulated DEGs found between vehicle-treated *Agl*^{-/-} mice and *Agl*^{-/-} mice receiving the AAV9-LiMP-GDEov treatment alone (**F**) or the combined AAV9-LiMP-GDEov-rapamycin treatment (**G**).

REFERENCES

1. Kishnani PS, Austin SL, Arn P, Bali DS, Boney A, Case LE, Chung WK, Desai DM, El-Gharbawy A, Haller R, et al. Glycogen storage disease type III diagnosis and management guidelines. *Genet Med.* 2010;12(7):446-63.

2. Sentner CP, Hoogeveen IJ, Weinstein DA, Santer R, Murphy E, McKiernan PJ, Steuerwald U, Beauchamp NJ, Taybert J, Laforet P, et al. Glycogen storage disease type III: diagnosis, genotype, management, clinical course and outcome. *J Inherit Metab Dis.* 2016;39(5):697-704.

3. Demo E, Frush D, Gottfried M, Koepke J, Boney A, Bali D, Chen YT, and Kishnani PS. Glycogen storage disease type III-hepatocellular carcinoma a long-term complication? *J Hepatol.* 2007;46(3):492-8.

4. Oterdoom LH, Verweij KE, Biermann K, Langeveld M, and van Buuren HR. Hepatocellular Adenomas and Carcinoma in Asymptomatic, Non-Cirrhotic Type III Glycogen Storage Disease. *J Gastrointestin Liver Dis.* 2015;24(4):515-8.

5. Ben Chehida A, Ben Messaoud S, Ben Abdelaziz R, Ben Ali N, Boudabous H, Ben Abdelaziz I, Ben Ameur Z, Sassi Y, Kaabachi N, Abdelhak S, et al. Neuromuscular Involvement in Glycogen Storage Disease Type III in Fifty Tunisian Patients: Phenotype and Natural History in Young Patients. *Neuropediatrics.* 2019;50(1):22-30.

6. Derks TG, and Smit GP. Dietary management in glycogen storage disease type III: what is the evidence? *J Inherit Metab Dis.* 2015;38(3):545-50.

7. Brambilla A, Mannarino S, Pretese R, Gasperini S, Galimberti C, and Parini R. Improvement of Cardiomyopathy After High-Fat Diet in Two Siblings with Glycogen Storage Disease Type III. *JIMD Rep.* 2014;17(91-5.

8. Dagli AI, Zori RT, McCune H, Ivsic T, Maisenbacher MK, and Weinstein DA. Reversal of glycogen storage disease type IIIa-related cardiomyopathy with modification of diet. *J Inherit Metab Dis.* 2009;32 Suppl 1(0 1):S103-6.

9. Valayannopoulos V, Bajolle F, Arnoux JB, Dubois S, Sannier N, Baussan C, Petit F, Labrune P, Rabier D, Ottolenghi C, et al. Successful treatment of severe cardiomyopathy in glycogen storage disease type III With D,L-3-hydroxybutyrate, ketogenic and high-protein diet. *Pediatr Res.* 2011;70(6):638-41.

10. Sentner CP, Caliskan K, Vletter WB, and Smit GP. Heart Failure Due to Severe Hypertrophic Cardiomyopathy Reversed by Low Calorie, High Protein Dietary Adjustments in a Glycogen Storage Disease Type IIIa Patient. *JIMD Rep.* 2012;5(13-6.

11. Olgac A, Inci A, Okur I, Biberoglu G, Oguz D, Ezgu FS, Kasapkara CS, Aktas E, and Tumer L. Beneficial Effects of Modified Atkins Diet in Glycogen Storage Disease Type IIIa. *Ann Nutr Metab.* 2020;76(4):233-41.

12. Mayorandan S, Meyer U, Hartmann H, and Das AM. Glycogen storage disease type III: modified Atkins diet improves myopathy. *Orphanet J Rare Dis.* 2014;9(196.

13. Colella P, Sellier P, Costa Verdera H, Puzzo F, van Wittenberghe L, Guerchet N, Daniele N, Gjata B, Marmier S, Charles S, et al. AAV Gene Transfer with Tandem Promoter Design Prevents Anti-transgene Immunity and Provides Persistent Efficacy in Neonate Pompe Mice. *Mol Ther Methods Clin Dev.* 2019;12(85-101.

14. Costa-Verdera H, Collaud F, Riling CR, Sellier P, Nordin JML, Preston GM, Cagin U, Fabregue J, Barral S, Moya-Nilges M, et al. Hepatic expression of GAA results in enhanced enzyme bioavailability in mice and non-human primates. *Nat Commun.* 2021;12(1):6393.

15. Demaster A, Luo X, Curtis S, Williams KD, Landau DJ, Drake EJ, Kozink DM, Bird A, Crane B, Sun F, et al. Long-term efficacy following readministration of an adeno-associated virus vector in dogs with glycogen storage disease type Ia. *Hum Gene Ther.* 2012;23(4):407-18.

16. Eggers M, Vannoy CH, Huang J, Purushothaman P, Brassard J, Fonck C, Meng H, Prom MJ, Lawlor MW, Cunningham J, et al. Muscle-directed gene therapy corrects Pompe disease and uncovers species-specific GAA immunogenicity. *EMBO Mol Med.* 2022;14(1):e13968.

17. Lee YM, Conlon TJ, Specht A, Coleman KE, Brown LM, Estrella AM, Dambska M, Dahlberg KR, and Weinstein DA. Long-term safety and efficacy of AAV gene therapy in the canine model of glycogen storage disease type Ia. *J Inherit Metab Dis.* 2018;41(6):977-84.

18. Puzzo F, Colella P, Biferi MG, Bali D, Paulk NK, Vidal P, Collaud F, Simon-Sola M, Charles S, Hardet R, et al. Rescue of Pompe disease in mice by AAV-mediated liver delivery of secretable acid alpha-glucosidase. *Sci Transl Med.* 2017;9(418).

19. Conlon TJ, Mah CS, Pacak CA, Rucker Henninger MB, Erger KE, Jorgensen ML, Lee CC, Tarantal AF, and Byrne BJ. Transfer of Therapeutic Genes into Fetal Rhesus Monkeys Using Recombinant Adeno-Associated Type I Viral Vectors. *Hum Gene Ther Clin Dev.* 2016;27(4):152-9.

20. Doerfler PA, Todd AG, Clement N, Falk DJ, Nayak S, Herzog RW, and Byrne BJ. Copackaged AAV9 Vectors Promote Simultaneous Immune Tolerance and Phenotypic Correction of Pompe Disease. *Hum Gene Ther.* 2016;27(1):43-59.

21. Fraites TJ, Jr., Schleissing MR, Shanely RA, Walter GA, Cloutier DA, Zolotukhin I, Pauly DF, Raben N, Plotz PH, Powers SK, et al. Correction of the enzymatic and functional deficits in a model of Pompe disease using adeno-associated virus vectors. *Mol Ther.* 2002;5(5 Pt 1):571-8.

22. Vidal P, Pagliarani S, Colella P, Costa Verdera H, Jauze L, Gjorgjieva M, Puzzo F, Marmier S, Collaud F, Simon Sola M, et al. Rescue of GSDIII Phenotype with Gene Transfer Requires Liver- and Muscle-Targeted GDE Expression. *Mol Ther.* 2018;26(3):890-901.

23. Lim JA, Choi SJ, Gao F, Kishnani PS, and Sun B. A Novel Gene Therapy Approach for GSD III Using an AAV Vector Encoding a Bacterial Glycogen Debranching Enzyme. *Mol Ther Methods Clin Dev.* 2020;18(240-9.

24. Lim JA, Kishnani PS, and Sun B. Suppression of pullulanase-induced cytotoxic T cell response with a dual promoter in GSD IIIa mice. *JCI Insight.* 2022;7(23).

25. Hakim CH, Kumar SRP, Perez-Lopez DO, Wasala NB, Zhang D, Yue Y, Teixeira J, Pan X, Zhang K, Million ED, et al. Cas9-specific immune responses compromise local and systemic AAV CRISPR therapy in multiple dystrophic canine models. *Nat Commun.* 2021;12(1):6769.

26. Yi H, Brooks ED, Thurberg BL, Fyfe JC, Kishnani PS, and Sun B. Correction of glycogen storage disease type III with rapamycin in a canine model. *J Mol Med (Berl).* 2014;92(6):641-50.

27. Franco LM, Sun B, Yang X, Bird A, Zhang H, Schneider A, Brown T, Young SP, Clay TM, Amalfitano A, et al. Evasion of immune responses to introduced human acid alpha-glucosidase by liver-restricted expression in glycogen storage disease type II. *Mol Ther.* 2005;12(5):876-84.

28. Zhang P, Sun B, Osada T, Rodriguiz R, Yang XY, Luo X, Kemper AR, Clay TM, and Koeberl DD. Immunodominant liver-specific expression suppresses transgene-directed immune responses in murine pompe disease. *Hum Gene Ther.* 2012;23(5):460-72.

29. Chandler RJ, LaFave MC, Varshney GK, Trivedi NS, Carrillo-Carrasco N, Senac JS, Wu W, Hoffmann V, Elkahloun AG, Burgess SM, et al. Vector design influences hepatic genotoxicity after adeno-associated virus gene therapy. *J Clin Invest.* 2015;125(2):870-80.

30. Mizushima N, Yoshimori T, and Levine B. Methods in mammalian autophagy research. *Cell.* 2010;140(3):313-26.

31. Laforet P, Inoue M, Goillot E, Lefeuvre C, Cagin U, Streichenberger N, Leonard-Louis S, Brochier G, Madelaine A, Labasse C, et al. Deep morphological analysis of muscle biopsies from type III glycogenesis (GSDIII), debranching enzyme deficiency, revealed stereotyped vacuolar myopathy and autophagy impairment. *Acta Neuropathol Commun.* 2019;7(1):167.

32. Shi X, Aronson SJ, Ten Bloemendaal L, Duijst S, Bakker RS, de Waart DR, Bortolussi G, Collaud F, Oude Elferink RP, Muro AF, et al. Efficacy of AAV8-hUGT1A1 with Rapamycin in neonatal, suckling, and juvenile rats to model treatment in pediatric CNs patients. *Mol Ther Methods Clin Dev.* 2021;20(287-97.

33. Ashe KM, Taylor KM, Chu Q, Meyers E, Ellis A, Jingozyan V, Klinger K, Finn PF, Cooper CG, Chuang WL, et al. Inhibition of glycogen biosynthesis via mTORC1 suppression as an adjunct therapy for Pompe disease. *Mol Genet Metab.* 2010;100(4):309-15.

34. Farah BL, Yen PM, and Koeberl DD. Links between autophagy and disorders of glycogen metabolism - Perspectives on pathogenesis and possible treatments. *Mol Genet Metab.* 2020;129(1):3-12.

35. Lim JA, Li L, Shirihai OS, Trudeau KM, Puertollano R, and Raben N. Modulation of mTOR signaling as a strategy for the treatment of Pompe disease. *EMBO Mol Med.* 2017;9(3):353-70.

36. Hosel M, Huber A, Bohlen S, Lucifora J, Ronzitti G, Puzzo F, Boisgerault F, Hacker UT, Kwanten WJ, Kloting N, et al. Autophagy determines efficiency of liver-directed gene therapy with adeno-associated viral vectors. *Hepatology.* 2017;66(1):252-65.

37. Ilyinskii PO, Michaud AM, Rizzo GL, Roy CJ, Leung SS, Elkins SL, Capela T, Chowdhury A, Li L, Chandler RJ, et al. ImmTOR nanoparticles enhance AAV transgene expression after initial and repeat dosing in a mouse model of methylmalonic acidemia. *Mol Ther Methods Clin Dev.* 2021;22(279-92.

38. Ilyinskii PO, Michaud AM, Roy CJ, Rizzo GL, Elkins SL, Capela T, Chowdhury AC, Leung SS, and Kishimoto TK. Enhancement of liver-directed transgene expression at initial and repeat doses of AAV vectors admixed with ImmTOR nanoparticles. *Sci Adv.* 2021;7(9).

39. Rusinova I, Forster S, Yu S, Kannan A, Masse M, Cumming H, Chapman R, and Hertzog PJ. Interferome v2.0: an updated database of annotated interferon-regulated genes. *Nucleic Acids Res.* 2013;41(Database issue):D1040-6.

40. Samarajiwa SA, Forster S, Auchettl K, and Hertzog PJ. INTERFEROME: the database of interferon regulated genes. *Nucleic Acids Res.* 2009;37(Database issue):D852-7.

41. Illingworth B, Cori GT, and Cori CF. Amylo-1, 6-glucosidase in muscle tissue in generalized glycogen storage disease. *J Biol Chem.* 1956;218(1):123-9.

42. Pursell N, Gierut J, Zhou W, Dills M, Diwanji R, Gjorgjieva M, Saxena U, Yang JS, Shah A, Venkat N, et al. Inhibition of Glycogen Synthase II with RNAi Prevents Liver Injury in Mouse Models of Glycogen Storage Diseases. *Mol Ther.* 2018;26(7):1771-82.

43. Meliani A, Boisgerault F, Hardet R, Marmier S, Collaud F, Ronzitti G, Leborgne C, Costa Verdera H, Simon Sola M, Charles S, et al. Antigen-selective modulation of AAV immunogenicity with tolerogenic rapamycin nanoparticles enables successful vector re-administration. *Nat Commun.* 2018;9(1):4098.

44. Butterfield JSS, Yamada K, Bertolini TB, Syed F, Kumar SRP, Li X, Arisa S, Pineros AR, Tapia A, Rogers CA, et al. IL-15 blockade and rapamycin rescue multifactorial loss of factor VIII from AAV-transduced hepatocytes in hemophilia A mice. *Mol Ther.* 2022;30(12):3552-69.

45. Xiang Z, Kuranda K, Quinn W, Chekaoui A, Ambrose R, Hasanpourghai M, Novikov M, Newman D, Cole C, Zhou X, et al. The Effect of Rapamycin and Ibrutinib on Antibody Responses to Adeno-Associated Virus Vector-Mediated Gene Transfer. *Hum Gene Ther.* 2022;33(11-12):614-24.

46. Perez-Iturralde A, Carte B, and Aldabe R. Consequences of Mammalian Target of Rapamycin Inhibition on Adeno-Associated Virus Hepatic Transduction Efficacy. *Hum Gene Ther.* 2021;32(19-20):1242-50.

47. Bartolo L, Li Chung Tong S, Chappert P, Urbain D, Collaud F, Colella P, Richard I, Ronzitti G, Demengeot J, Gross DA, et al. Dual muscle-liver transduction imposes immune tolerance for muscle transgene engraftment despite preexisting immunity. *JCI Insight.* 2019;4(11).

48. Poupiot J, Costa Verdera H, Hardet R, Colella P, Collaud F, Bartolo L, Davoust J, Sanatine P, Mingozzi F, Richard I, et al. Role of Regulatory T Cell and Effector T Cell Exhaustion in Liver-Mediated Transgene Tolerance in Muscle. *Mol Ther Methods Clin Dev.* 2019;15(83-100.

49. Byles V, Covarrubias AJ, Ben-Sahra I, Lamming DW, Sabatini DM, Manning BD, and Horng T. The TSC-mTOR pathway regulates macrophage polarization. *Nat Commun.* 2013;4(2834.

50. Mukhopadhyay S, Frias MA, Chatterjee A, Yellen P, and Foster DA. The Enigma of Rapamycin Dosage. *Mol Cancer Ther.* 2016;15(3):347-53.

51. Gardin A, and Ronzitti G. Current limitations of gene therapy for rare pediatric diseases: Lessons learned from clinical experience with AAV vectors. *Arch Pediatr.* 2023;30(8S1):8S46-8S52.

52. Ronzitti G, Gross DA, and Mingozzi F. Human Immune Responses to Adeno-Associated Virus (AAV) Vectors. *Front Immunol.* 2020;11(670.

53. Gardin A, Rouillon J, Montalvo-Romeral V, Rossiaud L, Vidal P, Launay R, Vie M, Krimi Benchekroun Y, Cosette J, Bertin B, et al. A functional mini-GDE transgene corrects impairment in models of glycogen storage disease type III. *J Clin Invest.* 2024;134(2).

54. Sellier P, Vidal P, Bertin B, Gicquel E, Bertil-Froidevaux E, Georger C, van Wittenberghe L, Miranda A, Daniele N, Richard I, et al. Muscle-specific, liver-detargeted adeno-associated virus gene therapy rescues Pompe phenotype in adult and neonate Gaa(-/-) mice. *J Inherit Metab Dis.* 2024;47(1):119-34.

55. Matsushita T, Elliger S, Elliger C, Podsakoff G, Villarreal L, Kurtzman GJ, Iwaki Y, and Colosi P. Adeno-associated virus vectors can be efficiently produced without helper virus. *Gene Ther.* 1998;5(7):938-45.

56. Ayuso E, Mingozzi F, and Bosch F. Production, purification and characterization of adeno-associated vectors. *Curr Gene Ther.* 2010;10(6):423-36.

57. Collaud F, Bortolussi G, Guianvarc'h L, Aronson SJ, Bordet T, Veron P, Charles S, Vidal P, Sola MS, Rundwasser S, et al. Preclinical Development of an AAV8-hUGT1A1 Vector for the Treatment of Crigler-Najjar Syndrome. *Mol Ther Methods Clin Dev.* 2019;12(157-74.

58. Leborgne C, Barbon E, Alexander JM, Hanby H, Delignat S, Cohen DM, Collaud F, Muraleetharan S, Lupo D, Silverberg J, et al. IgG-cleaving endopeptidase enables in vivo gene therapy in the presence of anti-AAV neutralizing antibodies. *Nat Med.* 2020;26(7):1096-101.

59. Schmieder R, and Edwards R. Quality control and preprocessing of metagenomic datasets. *Bioinformatics.* 2011;27(6):863-4.

60. Dobin A, Davis CA, Schlesinger F, Drenkow J, Zaleski C, Jha S, Batut P, Chaisson M, and Gingeras TR. STAR: ultrafast universal RNA-seq aligner. *Bioinformatics.* 2013;29(1):15-21.

61. Danecek P, Bonfield JK, Liddle J, Marshall J, Ohan V, Pollard MO, Whitwham A, Keane T, McCarthy SA, Davies RM, et al. Twelve years of SAMtools and BCFtools. *Gigascience.* 2021;10(2).

62. Anders S, Pyl PT, and Huber W. HTSeq--a Python framework to work with high-throughput sequencing data. *Bioinformatics.* 2015;31(2):166-9.

63. Love MI, Huber W, and Anders S. Moderated estimation of fold change and dispersion for RNA-seq data with DESeq2. *Genome Biol.* 2014;15(12):550.

64. Subramanian A, Tamayo P, Mootha VK, Mukherjee S, Ebert BL, Gillette MA, Paulovich A, Pomeroy SL, Golub TR, Lander ES, et al. Gene set enrichment analysis: a knowledge-based approach for interpreting genome-wide expression profiles. *Proc Natl Acad Sci U S A.* 2005;102(43):15545-50.

65. Wu T, Hu E, Xu S, Chen M, Guo P, Dai Z, Feng T, Zhou L, Tang W, Zhan L, et al. clusterProfiler 4.0: A universal enrichment tool for interpreting omics data. *Innovation (Camb).* 2021;2(3):100141.

66. Ashburner M, Ball CA, Blake JA, Botstein D, Butler H, Cherry JM, Davis AP, Dolinski K, Dwight SS, Eppig JT, et al. Gene ontology: tool for the unification of biology. The Gene Ontology Consortium. *Nat Genet.* 2000;25(1):25-9.

67. Kanehisa M, and Goto S. KEGG: kyoto encyclopedia of genes and genomes. *Nucleic Acids Res.* 2000;28(1):27-30.